Experimental mapping of the absolute magnitude of the transition dipole moment function $\mu_e(R)$ of the Na_2 $A\ ^1\Sigma_u^+ - X\ ^1\Sigma_g^+$ transition

E. H. Ahmed,[1] P. Qi,[1] B. Beser,[1] J. Bai,[1] R. W. Field,[2] J. P. Huennekens,[3] and A. M. Lyyra[1,*]
[1]*Physics Department, Temple University, Philadelphia, Pennsylvania 19122-6082, USA*
[2]*Chemistry Department, Massachusetts Institute of Technology, Cambridge, Massachusetts 02139, USA*
[3]*Department of Physics, 16 Memorial Drive East, Lehigh University, Bethlehem, Pennsylvania 18015, USA*
(Received 25 March 2008; published 29 May 2008)

The absolute magnitude of the transition dipole moment function $\mu_e(R)$ of the $A\ ^1\Sigma_u^+ - X\ ^1\Sigma_g^+$ band system of Na_2 was mapped experimentally over a relatively large range of internuclear distance R. The transition dipole moment matrix element of a set of rovibrational transitions between the $A\ ^1\Sigma_u^+$ and $X\ ^1\Sigma_g^+$ states was measured using the Autler-Townes effect. By employing the R-centroid approximation, or a fit to a polynomial function involving higher order R centroids, μ_e as a function of the internuclear distance was obtained. These Autler-Townes effect based measurements yield the absolute magnitude of μ_e, which can be used to test *ab initio* theoretical transition dipole moment functions or to "normalize" experimental transition moment functions obtained from intensity measurements, which in general give only the relative behavior of $\mu_e(R)$.

DOI: 10.1103/PhysRevA.77.053414 PACS number(s): 33.40.+f, 42.50.Hz

I. INTRODUCTION

Absolute intensities of molecular rovibronic transitions are of fundamental and general importance [1,2]. However, their accurate measurement has been very difficult traditionally. Compared to atomic systems, the internuclear distance dependence of molecular parameters such as the electronic transition dipole moment complicates the situation even further.

Recently it has been shown that quantum interference effects such as the Autler-Townes (AT) effect can be used to determine the absolute magnitude of the electronic transition dipole moment matrix element $\bar{\mu}_{v'J',v''J''} = \langle v', J' | \mu_e(R) | v'', J'' \rangle$ for a given rovibronic transition by determining the Rabi frequency $\Omega = \mu E/\hbar$ from the measured Autler-Townes splitting of a rovibronic transition and by measuring the coupling laser E field amplitude accurately [3–5]. In our earlier work we have demonstrated such a measurement for a specific rovibronic transition between the ground and the first excited states by using a four-level extended-Λ triple resonance excitation scheme [6–8]. By using this excitation scheme we explore here the possibility of determining the internuclear distance dependence of the electronic transition dipole moment function $\mu_e(R)$ for the Na_2 $A\ ^1\Sigma_u^+ - X\ ^1\Sigma_g^+$ system. For other electronic transitions, possible triple resonance excitation schemes are indicated in Ref. [7].

In principle, a simpler two-laser three-level cascade excitation scheme can be considered for such a study of transition dipole moments between the ground and the excited states. But, as has been shown in Ref. [6], that scheme is less favorable for a Doppler broadened sample with a thermal population distribution in the ground state. This is because the coupling laser transition from the ground state to the first excited state is Doppler broadened and the higher coupling laser power required to observe the AT splitting results in lower resolution due to saturation broadening. In addition, the available coupling laser Rabi frequencies are limited by the Franck-Condon factors available for excitations starting from the thermally populated levels of the ground state.

The four-level extended-Λ scheme shown in Fig. 1 overcomes these difficulties by dedicating separate lasers to the roles of the pump and coupling lasers. Thus a low power narrow band pump laser is used to select a narrow velocity group from the Doppler broadened transition as in Ref. [6] in order to enhance the resolution of the probe laser scan, the sole purpose of which is to reveal the Autler-Townes splitting of the intermediate level. The coupling laser can be tuned to resonance with transitions outside the thermally populated ground-state levels. Thus transitions with large transition dipole moment matrix elements, resulting in large Rabi frequencies, can be chosen for the coupling field, giving rise to a larger and better resolved AT splitting. The ability to

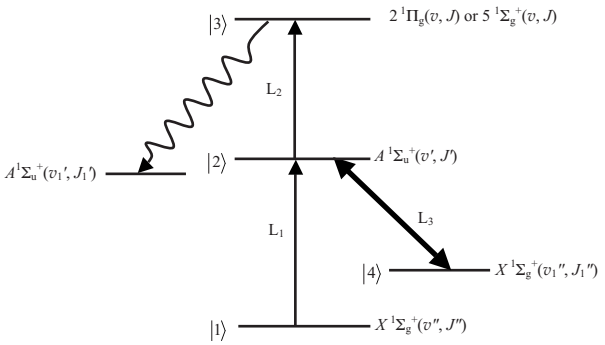

FIG. 1. Energy level diagram for the extended-Λ four level system with triple resonance excitation. The pump and probe lasers, L_1 and L_2, are in a copropagating arrangement and counterpropagate with the coupling field L_3. $|1\rangle$ denotes the initial level of L_1 $X\ ^1\Sigma_g^+(v'', J'')$; $|2\rangle$ denotes the intermediate state $A\ ^1\Sigma_u^+(v', J')$, which is the terminal level of L_1 and initial level of L_2; $|3\rangle$ denotes the upper state level to which the probe L_2 is tuned, namely, $2\ ^1\Pi_g(v, J)$ or $5\ ^1\Sigma_g^+(v, J)$; and $|4\rangle$ is the lower level $X\ ^1\Sigma_g^+(v_1'', J_1'')$ of the coupling field resonance transition.

*Author to whom correspondence should be addressed.

choose the coupling laser transition independently of the pump transition has the additional benefit of allowing measurements of transition dipole moments of a large number of rovibronic transitions between the ground and the excited states, which, as we demonstrate, can be used to construct the internuclear distance dependence of the electronic transition dipole moment $\mu_e(R)$.

Other traditional experimental methods to measure the variation of the transition dipole moment as a function of internuclear distance involve the measurement of either molecular fluorescence or absorption intensities [9–11], or the measurement of radiative lifetimes [12–14]. Absorption measurements and cavity ring down spectroscopy [15–17] are sensitive to the square of the transition dipole matrix element, but require knowledge of the initial state population in order to determine the absolute magnitude of the matrix element, and these methods are generally only useful for transitions out of thermally populated levels. Similarly, fluorescence intensity measurements can yield relative values of transition dipole matrix elements, if the wavelength and polarization dependence of the detection system efficiency is known. But obtaining absolute values of the transition dipole matrix elements from fluorescence intensity measurements requires not only the initial state populations, but also absolute intensity measurements, which are very difficult because of the need to calibrate the absolute detection system efficiency, the effective detection solid angle, etc. Lifetime measurements can yield absolute transition dipole matrix elements if all branching ratios can be determined.

In contrast to these difficulties, the critical measurements in the Autler-Townes splitting based method are the accurate measurement of the electric field amplitude E of the coupling laser and the Autler-Townes split fluorescence line profile [6]. This spectral line profile can then be used to determine the Rabi frequency $\Omega=\mu E/\hbar$, which directly yields the magnitude of the transition dipole moment matrix element $\bar{\mu}_{v'J',v''J''}=\langle v',J'|\mu_e(R)|v'',J''\rangle$. This matrix element represents an overlap integral of the rovibronic wave functions of the two levels weighted with the electronic transition dipole moment $\mu_e(R)$. In general the electronic transition moment function $\mu_e(R)$ between two electronic states in a diatomic molecule is a function of the internuclear distance R and in many cases this dependence can be very strong. In some cases only *ab initio* calculations are available for $\mu_e(R)$, but in most cases no information at all is available regarding the functional form of $\mu_e(R)$. While it is possible to test the accuracy of *ab initio* potential energy curves with high accuracy energy level measurements, it has been much harder to test theoretical transition dipole moments, because of the difficulties associated with the experimental measurement of their absolute magnitudes. A straightforward and accurate method to experimentally determine the absolute magnitude of the transition dipole moments of molecules as a function of internuclear distance simply has not been available especially over a wide range of R. Given this situation, it is common that an approximation is made by assuming that $\mu_e(R)$ is constant, or varies weakly as a function of R. Then the transition dipole moment integral is reduced to a simple vibrational overlap integral $\langle v'J'|v''J''\rangle$ times a constant of proportionality. The square of this vibrational overlap integral is the well-known Franck-Condon factor. The Franck-Condon factor is widely used for estimating relative transition strengths, but is only reliable when $\mu_e(R)$ does not change significantly in the R range of the transitions under consideration. However, if $\mu_e(R)$ strongly depends on R then one has to use the genuine $\langle v',J'|\mu_e(R)|v'',J''\rangle$ matrix element, highlighting the need for a method to obtain $\mu_e(R)$ from experimental measurements.

II. EXPERIMENT

Since the experimental setup and the excitation scheme are the same as reported in Ref. [6], we omit their detailed description here. For the labeling of the vibrational and rotational quantum numbers we use double prime and prime notation for the rovibrational levels from the ground and the first excited electronic states, respectively. Additionally, as all rotational levels of the $^1\Sigma^+$ electronic states are of e symmetry we will omit the e notation from the labeling of the $X\ ^1\Sigma_g^+$, $A\ ^1\Sigma_u^+$, and $5\ ^1\Sigma_g^+$ levels for simplicity. We will also omit the e/f symmetry notation for the rotational levels of the $2\ ^1\Pi_g$ state since the symmetry of the rotational levels of this state is determined by the rotational selection rules. For $^1\Pi_g \leftarrow {}^1\Sigma_u^+$ Q-branch transitions, only $f \leftrightarrow e$ transitions are allowed while for P and R branches only $e \leftrightarrow e$ transitions are allowed. In all cases during this experiment we have used only Q-branch transitions to the $2\ ^1\Pi_g$ state, and thus all rotational levels of the $2\ ^1\Pi_g$ state used in this work have f symmetry.

Figure 1 illustrates the energy level diagram of the extended-Λ excitation scheme. Lists of all pump, probe and coupling laser transition combinations used in the excitation scheme are given in Tables I and II. Our estimate for the accuracy of the laser wave numbers ($\tilde{\nu}=\omega/2\pi c$) listed in the tables is of the order of 0.01–0.02 cm^{-1}. This is due to the pump laser frequency drift (specified at 100 MHz/hour) during the experiment and the fact that the lasers were calibrated prior to the AT splitting measurement. The transition wave numbers $\tilde{\nu}$ for the pump, probe, and coupling transitions were calculated from the term values of the $X\ ^1\Sigma_g^+$ [18], $A\ ^1\Sigma_u^+$ [19], $5\ ^1\Sigma_g^+$ [20], and $2\ ^1\Pi_g$ [21] states. In all experiments we have verified that we are on resonance with the correct transitions. First the pump laser was checked by observing a resolved fluorescence spectrum to the ground state. Next the probe laser transition was verified by observing the OODR signal (by monitoring a specific rovibrational fluorescence decay channel of level $|3\rangle$) while it was scanned over the $2\ ^1\Pi_g(v,J) \leftarrow A\ ^1\Sigma_u^+(v',J')$ or $5\ ^1\Sigma_g^+(v,J) \leftarrow A\ ^1\Sigma_u^+(v',J')$ transition with the pump laser kept on resonance. Once the pump and probe transitions were verified the coupling laser was set exactly on resonance by observing the symmetric AT split spectrum from level $|3\rangle$.

The pump (L_1) and the probe (L_2) lasers were arranged in a copropagating configuration through the heat pipe oven. The coupling laser (L_3) counterpropagated relative to L_1 and L_2. The pump laser (L_1) was tuned to resonance on the $A\ ^1\Sigma_u^+(v',J') \leftarrow X\ ^1\Sigma_g^+(v'',J'')$ transition with the initial level within the thermal population range. In order to select a narrow velocity component within the Doppler profile, the power of L_1 was kept as low as possible while maintaining a

TABLE I. List of all pump, probe and coupling laser transition combinations used in the extended-Λ scheme with the probe transition to $5\ ^1\Sigma_g^+$. Our estimate for the accuracy of the laser wave numbers ($\tilde{\nu}$) is of the order of 0.01–0.02 cm^{-1}. This is due to the pump laser frequency drift (specified at 100 MHz/h) during the experiment and the fact that the lasers were calibrated prior to the AT splitting measurement. The spot size w_i and the power P_i of the lasers for the configurations in this table were as follows: $w_1=300$ μm, $P_1=0.4–0.8$ mW, $w_2=620$ μm, $P_2=1.7–3.0$ mW, $w_3=860$ μm and the power of the coupling laser P_3 was varied in the range of 200 to 700 mW in order to observe the power dependence of the AT splitting.

Pump laser L_1			Probe laser L_2			Coupling laser L_3		
$A\ ^1\Sigma_u^+$ (v',J')	$X\ ^1\Sigma_g^+$ (v'',J'')	$\tilde{\nu}_1$ (cm^{-1})	$5\ ^1\Sigma_g^+$ (v,J)	$A\ ^1\Sigma_u^+$ (v',J')	$\tilde{\nu}_2$ (cm^{-1})	$A\ ^1\Sigma_u^+$ (v',J')	$X\ ^1\Sigma_g^+$ (v_1'',J_1'')	$\tilde{\nu}_3$ (cm^{-1})
8,20	0,21	15545.855	9,21	8,20	17144.551	8,20	20,21	12694.648
10,20	1,21	15609.392	11,21	10,20	17126.074	10,20	17,21	13301.300
						10,20	20,21	12915.438
						10,20	23,21	12545.974
14,20	3,21	15732.128	15,21	14,20	17080.741	14,20	27,19	12523.406

reasonable signal to noise ratio in the AT split spectra. The Autler-Townes splitting of level $|2\rangle$, caused by the strong coupling laser L_3 on resonance with the transition $|2\rangle \leftrightarrow |4\rangle$ $[A\ ^1\Sigma_u^+(v',J') \leftrightarrow X\ ^1\Sigma_g^+(v_1'',J_1'')]$, was then detected in the fluorescence spectrum from level $|3\rangle$ as the weak probe laser (L_2) was scanned over the $2\ ^1\Pi_g(v,J) \leftarrow A\ ^1\Sigma_u^+(v',J')$ or $5\ ^1\Sigma_g^+(v,J) \leftarrow A\ ^1\Sigma_u^+(v',J')$ transition. Fluorescence of an isolated rovibronic transition (single channel $5\ ^1\Sigma_g^+ \rightarrow A\ ^1\Sigma_u^+$ or $2\ ^1\Pi_g \rightarrow A\ ^1\Sigma_u^+$ fluorescence) was used to monitor the population of the upper state $|3\rangle$. In all cases for level $|4\rangle$ we

TABLE II. List of all pump, probe and coupling laser transition combinations used in the extended-Λ scheme with probe transition to $2\ ^1\Pi_g$. The spot size w_i and the power P_i of the lasers for the configurations in this table were as follow: $w_1=570$ μm, $P_1=34$ mW, $w_2=510$ μm, $P_2=3–5$ mW, and $w_3=1185$ μm for the cases with intermediate level $A\ ^1\Sigma_u^+(v'=25,J'=20)$; $w_1=480$ μm, $P_1=13–15$ mW, $w_2=360$ μm, $P_2=3–5$ mW, and $w_3=1140$ μm for the cases with intermediate level $A\ ^1\Sigma_u^+(v'=28,J'=20)$; $w_1=600$ μm, $P_1=13–15$ mW, $w_2=300$ μm, $P_2=3–5$ mW, and $w_3=1140$ μm for the cases with intermediate level $A\ ^1\Sigma_u^+(v'=33,J'=20)$; $w_1=600$ μm, $P_1=15–30$ mW, $w_2=300$ μm, $P_2=3–5$ mW, and $w_3=960$ μm for the cases with intermediate levels $A\ ^1\Sigma_u^+(v'=34,J'=20)$ and $A\ ^1\Sigma_u^+(v'=35,J'=20)$. In all cases, P_3 was in the range of 200 to 700 mW.

Pump laser L_1			Probe laser L_2			Coupling laser L_3 (cm^{-1})		
$A\ ^1\Sigma_u^+$ (v',J')	$X\ ^1\Sigma_g^+$ (v'',J'')	$\tilde{\nu}_1$ (cm^{-1})	$2\ ^1\Pi_g$ (v,J)	$A\ ^1\Sigma_u^+$ (v',J')	$\tilde{\nu}_2$ (cm^{-1})	$A\ ^1\Sigma_u^+$ (v',J')	$X\ ^1\Sigma_g^+$ (v_1'',J_1'')	$\tilde{\nu}_3$ (cm^{-1})
25,20	1,19	17187.612	25,20	25,20	15519.884	25,20	38,20	12546.695
28,20	2,21	17313.617	28,20	28,20	15472.074	28,20	40,21	12673.775
						28,20	41,21	12594.436
						28,20	42,21	12518.021
						28,20	43,21	12444.657
33,20	5,19	17343.971	34,20	33,20	15462.944	33,20	43,19	12928.965
						33,20	43,21	12921.267
						33,20	46,19	12727.404
						33,20	48,21	12603.465
						33,20	51,21	12455.832
34,20	5,21	17424.924	36,20	34,20	15517.138	34,20	44,19	12951.722
						34,20	44,21	12944.247
						34,20	48,21	12696.658
35,20	6,21	17367.597	37,20	35,20	15496.524	35,20	45,19	12977.004

TABLE III. The experimentally determined transition dipole moment matrix elements μ_{exp} for the listed $A\ ^1\Sigma_u^+ - X\ ^1\Sigma_g^+$ rovibrational transitions with the corresponding R-centroid values of the electronic transition dipole moment μ_e and the values of the $\bar{R}$ and $\overline{R^2}$ centroids.

$A\ ^1\Sigma_u^+(v',J')$	$X\ ^1\Sigma_g^+(v'',J'')$	μ_{exp} (Debye)	$\mu_e(\bar{R})$ (Debye)	$\langle v'J'\vert v''J''\rangle$	$\bar{R}$ (Å)	$\overline{R^2}$ (Å^2)
8, 20	20, 21	3.10	10.03464	0.30893	4.17959	17.50138
10, 20	20, 21	2.54	9.77976	−0.25972	4.00123	16.00685
10, 20	17, 21	2.01	9.55051	0.21046	3.81830	14.59185
10, 20	23, 21	3.97	10.08869	0.39351	4.30459	18.55379
14, 20	27, 19	3.18	10.10133	0.31481	4.43664	19.76240
25, 20	38, 21	5.65	9.87193	0.57233	4.82040	23.39903
28, 20	42, 21	2.02	10.01885	−0.20162	4.56879	20.97709
28, 20	40, 21	3.40	9.92411	0.34260	5.28488	27.88646
28, 20	43, 21	3.33	10.05830	−0.33107	4.87420	23.81943
28, 20	41, 21	4.45	10.00900	0.44460	4.80207	23.28385
33, 20	43, 21	3.16	9.79298	0.32268	5.42271	29.47905
33, 20	43, 19	3.25	9.76445	0.33284	5.37345	29.01484
33, 20	46, 19	2.94	9.90332	−0.29687	5.13457	26.52676
33, 20	48, 21	3.38	9.98552	0.33849	4.78567	23.13510
33, 20	51, 21	2.10	10.10587	0.20780	4.91193	24.18479
34, 20	44, 21	2.64	9.74134	0.27101	5.60201	31.21213
34, 20	44, 19	2.80	9.73168	0.28772	5.53629	30.58911
34, 20	48, 21	1.95	9.89546	0.19706	5.27048	27.76312
35, 20	45, 19	1.82	9.75505	0.18657	5.81283	33.25829

have chosen a high vibrational level of the ground state, outside the range of the thermally populated levels.

The pump laser L_1 and the probe laser L_2 were Coherent Autoscan 699-29 dye lasers operating either with DCM or R6G dye, while the coupling laser, L_3, was a Coherent Autoscan 899-29 titanium sapphire laser. The laser beams have a Gaussian distribution $\text{TEM}_{0,0}$ transverse profile characterized by the spot size w_i (for the ith laser), defined here as the diameter measured at $1/e^2$ of the peak intensity. We denote the total power of the ith laser with P_i. By varying the low power levels of lasers L_1 and L_2 we found the best combination of these parameters for the chosen laser beam spot sizes by making sure that this choice had a minimal effect on the observed AT splitting spectra while still resulting in an acceptable signal to noise ratio. To verify the linear dependence of the measured AT splitting on the coupling laser E field amplitude in the level $\vert 3\rangle$ fluorescence excitation spectra, the power of the pump and probe lasers was kept constant, while the power of the coupling laser was varied, generally between 200 and 700 mW, by using neutral density filters.

The simulations of the experimentally recorded AT split spectra were performed using the density matrix formalism outlined in Refs. [6,8] with the following parameters: lifetime of the $A\ ^1\Sigma_u^+(v',J')$ levels, $\tau_2=12.5$ ns [22]; lifetime of the $2\ ^1\Pi_g(v,J)$ levels, $\tau_3=18.3$ ns [6] and the lifetime of the $5\ ^1\Sigma_g^+$ levels is $\tau_3=40.3$ ns; branching ratios W_{32}/W_3, W_{21}/W_2, W_{24}/W_2 calculated from the corresponding Franck-Condon factors; sample temperature of approximately 600 K and its corresponding Doppler width; collisional dephasing rates $\gamma_{12}/2\pi=\gamma_{24}/2\pi=\gamma_{14}/2\pi=\gamma_{13}/2\pi=\gamma_{23}/2\pi=\gamma_{34}/2\pi=4.77$ MHz; transit relaxation rate $w_t/2\pi=0.38$ MHz. The various excitation and decay processes in the excitation scheme for each combination of pump, probe, and coupling transitions were taken into account in the density matrix simulations in the same fashion as in Ref. [6]. The simulations included averaging over the molecular velocity distribution, summation over the magnetic sublevels m_J, and averaging over the radial distribution of the electric fields of the lasers. The Rabi frequency of the coupling field Ω_3 was varied until the best fit to the recorded experimental spectrum was obtained. The resulting Ω_3 value along with the strength of the coupling laser electric field E_3 was used to calculate the transition dipole moment matrix element between the rovibrational levels coupled by E_3. For calculating the coupling laser electric field amplitude we used the formula $E_3=\sqrt{2/c\epsilon_0}\sqrt{8P_3/\pi w_3^2}$. The main contributions to the error in the electric field determination arise from the experimental errors in the measurements of the spot size w_3 and the total laser power P_3. From the definition of the Rabi frequency $\Omega=\mu E_0/\hbar$ the transition dipole moment matrix elements for the coupling transitions were determined. However, it should be noted that this method cannot determine the sign of the dipole matrix element. The resulting transition dipole moment matrix elements μ_{exp} are given in Table III. These values are an average of the transition dipole moment matrix elements determined from a number of spectra (5 to 10 individual spectra with different coupling laser powers) for the particular coupling transition. We estimate that the uncertainty in the value of μ_{exp} is about ± 0.2 Debye, arising mainly from the error in the measurement of the spot sizes (± 10 μm), the laser power fluctuation (1–2 %), the abso-

lute power calibration of our power meter, and the inherent noise in the recorded spectra.

In order to compare this Autler-Townes splitting method of measuring the R-dependent absolute transition dipole moment function with the more traditional method of determining the relative R dependence, we have also carried out a series of resolved fluorescence scans. The Coherent 699-29 dye laser, using R6G or DCM dye, was tuned to line center of the $A\ ^1\Sigma_u^+(v'=35,J'=20)\leftarrow X\ ^1\Sigma_g^+(v''=5,J''=21)$, $A\ ^1\Sigma_u^+(v'=34,J'=20)\leftarrow X\ ^1\Sigma_g^+(v''=5,J''=21)$, $A\ ^1\Sigma_u^+(v'=25,J'=20)\leftarrow X\ ^1\Sigma_g^+(v''=1,J''=19)$, $A\ ^1\Sigma_u^+(v'=20,J'=20)\leftarrow X\ ^1\Sigma_g^+(v''=1,J''=21)$, and $A\ ^1\Sigma_u^+(v'=10,J'=20)\leftarrow X\ ^1\Sigma_g^+(v''=4,J''=21)$ transitions. In each case, fluorescence was collected from one of the side arms of the heat pipe oven and resolved with a Spex 0.85 m double-grating monochromator. The detection system, consisting of a monochromator and a photomultiplier tube (PMT), is known to display strong wavelength and polarization dependence [23]. Therefore a linear polarizer, oriented to pass horizontally polarized light, was placed in front of the monochromator. The detection system efficiency vs wavelength for horizontally polarized light was determined [23] using a calibrated tungsten-halogen lamp [24], and the resolved spectra were corrected for this. Total $A\ ^1\Sigma_u^+(v',J')\rightarrow X\ ^1\Sigma_g^+$ fluorescence was continuously monitored through the opposite side arm to identify and correct for any drift of the laser frequency from line center of the pump transition during the ~30 min. resolved fluorescence scan.

III. ELECTRONIC TRANSITION DIPOLE MOMENT FUNCTION $\mu_e(R)$

In this section we calculate the internuclear distance dependence of $\mu_e(R)$ from the set of experimentally measured transition dipole matrix elements μ_{exp}. For this purpose, either the simple R-centroid approximation, or a more complete polynomial expression that includes higher order R-centroids can be used [25–29].

If we represent $\mu_e(R)$ by a power series in the internuclear distance R

$$\mu_e(R)=\sum_{i=0}^{\infty}\mu_i R^i, \tag{1}$$

then the transition dipole moment matrix element can be written as

$$\langle v'|\mu_e(R)|v''\rangle=\langle v'|v''\rangle\sum_{i=0}^{\infty}\mu_i\overline{R^i}, \tag{2}$$

where $\langle v'|v''\rangle$ is the vibrational overlap integral, and $\overline{R^i}$ is the ith R centroid defined as

$$\overline{R^i}=\frac{\langle v'|R^i|v''\rangle}{\langle v'|v''\rangle}. \tag{3}$$

If we limit ourselves to the lowest order in Eq. (1) we obtain the Condon approximation [30] in which the matrix element is simply proportional to the vibrational overlap integral, equivalent to the root square of the Franck-Condon factor.

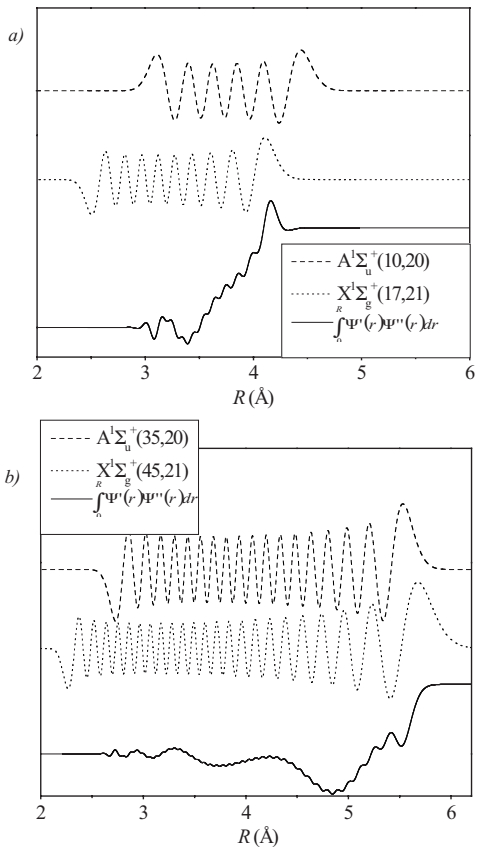

FIG. 2. Plots of the excited $A\ ^1\Sigma_u^+(v',J')$ and ground $X\ ^1\Sigma_g^+(v'',J'')$ state wave functions ψ' and ψ'' and of the overlap integral $\int_0^R\psi'(r)\psi''(r)dr$ as functions of the internuclear distance R for the cases (a) $A\ ^1\Sigma_u^+(10,20)$-$X\ ^1\Sigma_g^+(17,21)$ and (b) $A\ ^1\Sigma_u^+(35,20)$-$X\ ^1\Sigma_g^+(45,21)$.

In the R-centroid approximation [25–29]

$$\langle v'|\mu_e(R)|v''\rangle\approx\langle v'|v''\rangle\mu_e(\bar{R}), \tag{4}$$

the matrix element is approximated with the product of μ_e at the R-centroid value $\bar{R}$ and the overlap integral $\langle v'|v''\rangle$. By expanding $\mu_e(\bar{R})$ in a power series in $\bar{R}$, and approximating $\bar{R}^i$ with $\overline{R^i}$, Eq. (4) becomes equivalent to Eq. (2). It is easy to show that the R-centroid approximation becomes exact when $\mu_e(R)$ is a linear function of R.

The R-centroid method is adequate in cases where there is only a single classical turning point, as is the case shown in Fig. 2(a), where the calculated R-centroid value of 3.82 Å corresponds closely to the center of the interval from 3.5 to 4.2 Å where most of the value of the overlap integral accumulates. On the other hand in cases where the integral accumulates over a large interval of R, as shown in Fig. 2(b), the method is unreliable. In such cases, Eq. (2) must be used to fit the experimentally obtained set of transition dipole moment matrix elements. Usually, truncation at the quadratic or cubic terms in the expansion is sufficient to represent the experimental data. Using a polynomial expansion of the electronic transition dipole moment up to second order in R,

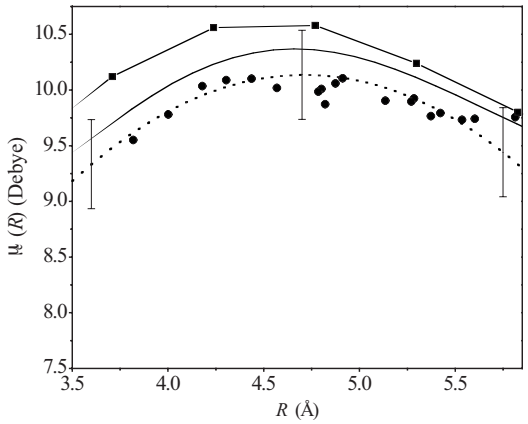

FIG. 3. Comparison between the transition dipole moment functions $\mu_e(R)$ obtained from experimental data and from *ab initio* calculations of Magnier [6] (solid line with squares) and Kotochigova [6] (solid line). The results from the *R*-centroid method are given as solid circular dots and the results from the fit with a quadratic polynomial expansion $\mu_e(R)=\mu_0+\mu_1 R+\mu_2 R^2$, with coefficients $\mu_0=-4.2502$ Debye, $\mu_1=6.1046$ Debye/Å, and $\mu_2=-0.64758$ Debye/Å^2 are given as a dashed line.

$$\mu_e(R) = \mu_0 + \mu_1 R + \mu_2 R^2, \tag{5}$$

we have fitted the experimental data for μ_{exp} from Table III and obtained the following values for the coefficients $\mu_0=-4.2502$ Debye, $\mu_1=6.1046$ Debye/Å, and $\mu_2=-0.64758$ Debye/Å^2. The values of the $\bar{R}$ and $\overline{R^2}$ centroids for the corresponding transitions used in the fitting procedure are given in Table III. We have calculated them using the computer program LEVEL 7.7 by Le Roy [31] with potentials for the *X* state and the *A* state from Refs. [18] and [19], respectively. The range in *R* within which $\mu_e(R)$ obtained from the fitting remains valid is determined by the extent of the range of the individual transition overlap integrals. The results for μ_e obtained using the simple *R*-centroid approximation given by Eq. (4) are listed in Table III as $\mu_e(\bar{R})$. $\mu_e(R)$ from Eq. (5) is illustrated in Fig. 3 (dotted line), while the results from the *R*-centroid approximation are represented by solid circles. For comparison, results from *ab initio* calculations of the electronic transition dipole moment $\mu_e(R)$ for the $A\ ^1\Sigma_u^+$-$X\ ^1\Sigma_g^+$ system are also shown [6,32]. The results of Magnier [32], represented with connected solid square symbols, are based on configuration interaction (CI) calculations in the framework of a pseudopotential method. The theoretical transition moment function of Kotochigova [6,33], represented with the solid line, is based on the relativistic configuration interaction valence bond method.

In our case there is no significant difference in the results for $\mu_e(R)$ obtained using the *R*-centroid method and by using the polynomial Eq. (5) based fit of the experimental results. This is because the coupling transitions used in the experiments were deliberately chosen in such a way (with a few exceptions) that the *R*-centroid approximation would be as accurate as possible for the corresponding range of internuclear distances.

Finally, in Fig. 4 we compare the absolute $\mu_e(R)$ function obtained here with the relative $\mu_e(R)$ function obtained from the resolved fluorescence measurements using the method described in Ref. [10] and the potentials of Refs. [18] and [19]. Individual $A\ ^1\Sigma_u^+(v',J') \rightarrow X\ ^1\Sigma_g^+(v'',J'')$ fluorescence line intensities are proportional to $\nu^4 |\langle v',J'|\mu_e(R)|v'',J''\rangle|^2$. However, in this case, using a fitting function of the form given in Eq. (5), we can only determine the ratios $\mu_1/\mu_0=-0.752$ Å^{-1} and $\mu_2/\mu_0=0.0808$ Å^{-2}. Because the fluorescence measurements yield only a relative transition dipole moment, this function is normalized to the average absolute measurement over the common range of *R*. Clearly, the absolute and relative measurements display the same basic *R* dependence, although the latter shows somewhat more curvature. The range of *R* covered by the relative fluorescence intensity measurements is limited by the inner and outer turning points 2.68 and 5.62 Å, respectively, of the highest $A\ ^1\Sigma_u^+$ state level investigated ($v'=35$, $J'=20$). Thus we see that the relative fluorescence intensity measurements can be used to extend $\mu_e(R)$ toward smaller *R*. However, we have found that the fluorescence measurements are not very sensitive to the dipole moment for *R* values below 3.0 Å, so only the region $R>3.0$ Å above this point is reported in Fig. 4. In a forthcoming paper [34], we will demonstrate how the combination of absolute measurements of $\bar{\mu}_{v'J',v''J''}=\langle v',J'|\mu_e(R)|v'',J''\rangle$ for selected rovibronic transitions, using Autler-Townes splitting, can be combined with fluorescence measurements to map strong *R* dependences of $\mu_e(R)$ for multiple electronic transitions.

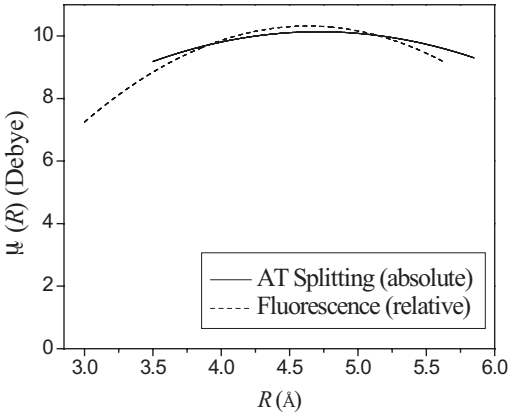

FIG. 4. Comparison of the absolute $\mu_e(R)$ function obtained using the Autler-Townes splitting method with the relative $\mu_e(R)$ function obtained from resolved fluorescence intensity measurements.

IV. CONCLUSIONS

We have presented a novel method to determine the internuclear distance dependence of the molecular electronic transition dipole moment. This technique uses the Autler-Townes quantum interference effect for measurement of the absolute magnitude of the transition dipole moment matrix element for molecular transitions between the ground and the excited states. Our results indicate that the extended-Λ excitation scheme is preferable for the moderate coupling field Rabi frequencies available with continuous wave laser sources. In this particular case, probing the transition dipole moment

between the ground state and an excited state, we have chosen the lower level of the coupling field from outside the thermal population range. Such vibrational levels with large wave function amplitudes at the outer turning point of the molecular vibration lead to large transition dipole moment matrix elements and, as a result, to larger Rabi frequencies for the coupling laser transitions. In addition, compared to a simpler three-level excitation scheme, which is limited to the internuclear distance range of the thermal population, the weak pump laser also defines a much narrower velocity group within the Doppler profile, leading to a better resolved AT splitting of the intermediate level.

By using the extended-Λ excitation scheme we have "tuned" the coupling laser to different rovibronic transitions in order to determine the internuclear distance dependence of the transition dipole moment function in the region defined by the overlap integrals of the coupling laser transitions. We have measured $|\langle v',J'|\mu_e(R)|v'',J''\rangle|$ for a number of transitions between the $A\ ^1\Sigma_u^+$ excited and $X\ ^1\Sigma_g^+$ ground states of a Na_2 Doppler broadened sample. We have calculated the internuclear distance dependence of the electronic transition dipole moment $\mu_e(R)$ from the experimentally determined set of $|\langle v',J'|\mu_e(R)|v'',J''\rangle|$ values, using both the R-centroid approximation and a polynomial expansion based on higher order R centroids.

ACKNOWLEDGMENT

This work was supported by National Science Foundation Grant No. PHY 0555608.

[1] G. H. Herzberg, *Molecular Spectra and Molecular Structure I. Spectra of Diatomic Molecules* (Van Nostrand, Princeton, 1950).
[2] A. C. G. Mitchell and M. W. Zemansky, *Resonance Radiation and Excited Atoms* (Cambridge University Press, Cambridge, 1971).
[3] M. A. Quesada, A. M. F. Lau, D. H. Parker, and D. W. Chandler, Phys. Rev. A **36**, 4107 (1987).
[4] J. Qi, F. C. Spano, T. Kirova, A. Lazoudis, J. Magnes, L. Li, L. M. Narducci, R. W. Field, and A. M. Lyyra, Phys. Rev. Lett. **88**, 173003 (2002).
[5] R. Garcia-Fernandez, A. Ekers, J. Klavins, L. P. Yatsenko, N. B. Bezuglov, B. W. Shore, and K. Bergmann, Phys. Rev. A **71**, 023401 (2005).
[6] E. Ahmed, A. Hansson, P. Qi, T. Kirova, A. Lazoudis, S. Kotochigova, A. M. Lyyra, L. Li, J. Qi, and S. Magnier, J. Chem. Phys. **124**, 084308 (2006).
[7] A. M. Lyyra, H. Wang, T.-J. Whang, W. C. Stwalley, and L. Li, Phys. Rev. Lett. **66**, 2724 (1991).
[8] E. Ahmed, Ph.D. thesis, Temple University, 2007 (unpublished).
[9] M. M. Hessel, E. W. Smith, and D. E. Drullinger, Phys. Rev. Lett. **33**, 1251 (1974).
[10] E. Laub, I. Mazsa, S. C. Webb, J. LaCivita, I. Prodan, Z. J. Jabbour, R. K. Namiotka, and J. Huennekens, J. Mol. Spectrosc. **193**, 376 (1999); **221**, 142(E) (2003).
[11] M. Lamrini, R. Bacis, D. Cerny, S. Churassy, P. Crozet, and A. J. Ross, J. Chem. Phys. **100**, 8780 (1994).
[12] J. Brzozowski, N. Elander, P. Erman, and M. Lyyra, Astrophys. J. **193**, 741 (1974).
[13] M. Tamanis, M. Auzinsh, I. Klincare, O. Nikolayeva, R. Ferber, A. Zaitsevskii, E. A. Patzyuk, and A. V. Stoloyarov, J. Chem. Phys. **109**, 6725 (1998).
[14] P. Erman, Astrophys. J. **213**, L89 (1977).
[15] A. O'Keefe and D. A. G. Deacon, Rev. Sci. Instrum. **59**, 2544 (1988).
[16] D. Romanini and K. K. Lehmann, J. Chem. Phys. **99**, 6287 (1993).
[17] J. J. Scherer, J. B. Paul, A. O'Keefe, and R. J. Saykally, Chem. Rev. **97**, 25 (1997).
[18] O. Babaky and K. Hussein, Can. J. Phys. **67**, 9112 (1989).
[19] P. Qi, J. Bai, E. Ahmed, A. M. Lyyra, S. Kotochigova, A. J. Ross, C. Effantin, P. Zalicki, J. Vigue, G. Chawla, R. W. Field, T.-J. Whang, W. C. Stwalley, L. Li, and T. Bergeman, J. Chem. Phys. **127**, 044301 (2007).
[20] C.-C. Tsai, J. T. Bahns, and W. C. Stwalley, J. Chem. Phys. **100**, 768 (1994).
[21] T.-J. Whang, H. Wang, A. M. Lyyra, L. Li, and W. C. Stwalley, J. Mol. Spectrosc. **145**, 112 (1991).
[22] G. Baumgartner, H. Kornmeier, and W. Preuss, Chem. Phys. Lett. **107**, 13 (1984).
[23] H. Chen, L. Li, G. Lazarov, X. Wang, A. M. Lyyra, J. Huennekens, and R. W. Field, J. Mol. Spectrosc. **196**, 197 (1999).
[24] R. Stair, W. E. Schneider, and J. K. Jackson, Appl. Opt. **2**, 1151 (1963).
[25] P. A. Fraser, Can. J. Phys. **32**, 515 (1954).
[26] J. Tellinghuisen, J. Mol. Spectrosc. **103**, 455 (1984).
[27] J. Tellinghuisen, in *Photodissociation and Photoionization*, edited by K. P. Lawley (Wiley, New York, 1985), pp. 299–369, and references therein.
[28] C. Noda and R. N. Zare, J. Mol. Spectrosc. **95**, 254 (1982).
[29] H. Lefebvre-Brion and R. W. Field, *The Spectra and Dynamics of Diatomic Molecules* (Elsevier, Amsterdam, 2004).
[30] E. U. Condon, Phys. Rev. **32**, 858 (1928).
[31] R. J. Le Roy (unpublished).
[32] S. Magnier, P. Millié, O. Dulieu, and F. Masnou-Seeuws, J. Chem. Phys. **98**, 7113 (1993).
[33] S. Kotochigova, E. Tiesinga, and I. Tupitsyn, *New Trends in Quantum Systems in Physics and Chemistry* (Kluwer Academic, The Netherlands, 2001), Vol. 1.
[34] S. J. Sweeney, E. Ahmed, P. Qi, A. M. Lyyra, and J. Huennekens (unpublished).